JCTC Journal of Chemical Theory and Computation

Article

pubs.acs.org/JCTC

Molecular Dynamics Simulations of Star Polymeric Molecules with Diblock Arms, a Comparative Study

William C. Swope,*[,†] Amber C. Carr,[‡] Amanda J. Parker,[§,∥] Joseph Sly,[†] Robert D. Miller,[†] and Julia E. Rice[†]

[†]IBM Research, IBM Almaden Research Center, San Jose, California 95120, United States

[‡]Department of Chemistry and Laufer Center for Physical and Quantitative Biology, Stony Brook University, Stony Brook, New York, United States

[§]MacDiarmid Institute for Advanced Materials and Nanotechnology, School of Chemical and Physical Sciences, Victoria University of Wellington, Wellington, New Zealand

ABSTRACT: We have performed all atom explicit solvent molecular dynamics simulations of three different star polymeric systems in water, each star molecule consisting of 16 diblock copolymer arms bound to a small adamantane core. The arms of each system consist of an inner "hydrophobic" block (either polylactide, polyvalerolactone, or polyethylene) and an outer hydrophilic block (polyethylene oxide, PEO). These models exhibit unusual structure very close to the core (clearly an artifact of our model) but which we believe becomes "normal" or bulk-like at relatively short distances from this core. We report on a number of temperature-dependent thermodynamic (structural/energetic) properties as well as kinetic properties. Our observations suggest that under physiological conditions, the hydrophobic regions of these systems may be solid and glassy, with only rare and shallow penetration by water, and that a sharp boundary exists between the hydrophobic cores and either the PEO or water. The PEO in these models is seen to be fully water-solvated at low temperatures but tends to phase separate from water as the temperature is increased, reminiscent of a lower critical solution temperature exhibited by PEO−water mixtures. Water penetration concentration and depth is composition and temperature dependent with greater water penetration for the most ester-rich star polymer.

1. INTRODUCTION

There is growing interest in the use of biocompatible polymeric nanoparticles for drug delivery. The hope is that such materials can be engineered to absorb therapeutic (drug) molecules before their delivery into the body and then to release them in a controlled or programmed manner under physiological conditions. Moreover, such nanoparticles could be functionalized on their exteriors to adhere to the membranes of cells of particular tissue types, or even to cells in a particular disease state. Such targeted delivery systems would result in much more effective therapies than can be achieved by normal means, with a consequent lowering of dosage and reduction of potential side effects.

Polymer chemists have shown amazing ingenuity[1−3] in producing polymers for these types of applications using complex sequences of monomeric units (e.g., diblock, triblock copolymers, and/or random copolymers) with various types of chemical functionality, a range of topologies, and various types and amounts of covalent and noncovalent cross-linking. Candidate nanoparticles under consideration for drug delivery include micelle and vesicle assemblies made from polymers and polymer blends,[4,5] as well as unimolecular systems with dendritic[6] and star[3] topologies and nanogel star polymers,[1,2] which have polymeric arms emanating from a nanogel core. Molecular systems with star, nanogel star, and dendritic topologies show promise over molecular assemblies because, being entirely covalently bonded, they are much more likely to be structurally stable over the range of environmental conditions seen in a living organism. However, all of these systems may be useful under different contexts or for different applications.

Of particular interest in this area is the design of *general purpose* vehicular nanoparticles where, with a relatively small range of chemical or topological variation, one would be able to engineer the delivery of a potentially large number of different types of cargo molecules, to provide precise control of their release rate and/or target delivery site or to transport multiple drug types simultaneously. To enable these types of functional variation using, for example, a star polymer topology, the polymer chemist has the freedom to change the number and length of the arms, and each arm may itself be a diblock or triblock polymer with different segment lengths. Furthermore, with nanogel star polymers, the arms of such a molecule do not all need to be identical in length and composition. Through variation of these features, a polymer chemist can, in principle, design nanogel star molecules with multiple compartments tailored for different types of cargo.

We are reminded that star polymer *topologies* exist in much broader classes of materials than just those with small molecule, dendritic, or nanogel core junctions, such as in the case of polymer-coated gold nanoparticles.[7,8] Even micelles, though not chemically bound, can have polymer−solvent interactions that bear a strong resemblance to those of the star polymers.

Special Issue: Wilfred F. van Gunsteren Festschrift

Received: March 6, 2012
Published: May 14, 2012

dx.doi.org/10.1021/ct300188e | J. Chem. Theory Comput. 2012, 8, 3733−3749

Star polymers can be synthesized and modeled with much smaller molecular systems yet can serve as useful and characterizable models for the polymeric structure and solvent−nanoparticle interactions of these more complex systems.

This paper concerns the study of an important class of polymeric nanoparticle, namely, the star polymer topology where each arm of the star is itself a diblock copolymer. In general, each arm of these molecules consists of a "hydrophobic" region positioned close to the interior of the star and a "hydrophilic" region on the exterior that serves to make the molecule water-soluble and prevent aggregation at finite concentrations.

Because of their use in a number of commercial application areas, star polymers have been studied extensively from both a theoretical and an experimental perspective. Comprehensive reviews have been developed by Grest et al.[9] as well as by Likos.[10] Both of these reviews also provide numerous references to a large body of Monte Carlo and molecular dynamics simulation studies, most of which have employed coarse grained (e.g., beaded string) models with intramolecular interactions designed to model good and poor solvents in an implicit way. These simulations have been very useful in helping to interpret experimental results and to validate theoretical scaling laws that describe the relationship, for example, between the radius of gyration and chain number and length in various qualities of solvent. On the other hand, the literature of all atom and explicit solvent simulations of star polymers is relatively sparse, particularly for star polymers with diblock arms. Ganazzoli et al.[11] used Monte Carlo techniques and a mean field type of approach to determine how the arms of a star polymer might behave in a generic poor solvent. Chang et al.[12] studied heteroarm copolymers, with some arms purely hydrophobic and some hydrophilic. Lee and Larson[13,14] used coarse grained molecular dynamics to model star polymers with a range of arm numbers and lengths with relatively long polyethylene oxide (PEO) arms bound to different sizes of dendrimeric cores.

The work most relevant to this study is that of Huynh et al.,[15] from the group of Prof. Christine Allen. They reported on a set of all atom explicit solvent simulations of six arm star polymers that explored the effect of varying the lengths of the hydrophobic and hydrophilic segments of each diblock arm made from polycaprolactone (PCL, a polyester with five methylene groups between ester groups) and PEO. Each of the six arms was attached to one of the terminal carbon atoms of diethylether. Using the OPLS force field[16,17] (much like the work reported here) and the SPC[18] water model, they studied 13 arm length variants, each with long simulations (200 ns) at 300 K, and were able to establish several important scaling relationships. In their simulations, they observed that the hydrophobic material is densely packed and excludes both water and the hydrophilic material (i.e., strongly segregated or phase separated), with a well-defined boundary between the hydrophobic material and water. Also, the PEO is highly mobile and adopts disordered conformations, and it is well solvated. If the PEO segments are short, the densely packed hydrophobic region is somewhat solvent exposed. However, as the length of the PEO segments is increased, the fractional coverage of the hydrophobic core by PEO increases, providing "protection" from water, leading them to suggest that sufficiently long PEO segments might inhibit aggregation in solutions of star copolymers at higher concentrations.

The main goal of this paper is to investigate the effect on the diblock star polymer structure, stability, and kinetics of changes in the hydrophobic region. The work examines three different polymers for the construction of the hydrophobic region of each diblock arm: polylactic acid (PLA), polyvalerolactone (PVL), and polyethylene (PE). These differ in the amount of ester versus alkane content, with PLA being the most rich in ester functional groups and the least rich in alkane, and PE being the least rich in ester (none) and most rich in alkane. The alkane component provides flexibility as well as hydrophobicity due to its nonpolar nature. Ester groups, in contrast, have an effective charge distribution that produces relatively strong electrostatic interactions, and the hydrophobicity of ester-rich polymers is due to their stronger attraction to other ester groups than to water, causing them to "phase separate" from water: the ester-rich condensate being more stable than water-solvated conformations. We note that PVL is very similar to the polycaprolactone (PCL) studied by Huynh et al.,[15] having four methylene groups between ester groups, one less than PCL.

The star polymers studied in this work have arms that are bound to a small adamantane junction. Star polymers with an adamantane junction have actually been synthesized, as reported by Huang et al.[19] The star polymers they prepared had four arms, compared with our 16, and theirs consisted of different polymeric materials, including styrenes and methacrylates. The four arms on their star polymers were not copolymers, and they were much longer than the ones we have simulated. We wish to emphasize at the outset, however, that our study is not meant to be about any particular adamantane-based star polymer. We are merely using this type of junction to attempt to generate a *model* that at an identified ("post-transitional") distance from the junction will be useful to help understand much larger star polymers of a similar composition.

This study makes use of fixed charge force fields, where a single charge model is used regardless of the environment in which an atom is situated. This is clearly an approximation since, from the physics of the situation, one would expect electronic polarization for a molecule that depends to a degree upon its environment. Even simple reaction field theory,[20] for example, predicts that the surrounding solvent causes an enhancement of the polarization of a molecule that depends on the dielectric constant of the solvent. One might reasonably expect, therefore, that the appropriate charge model to use for an ester surrounded by water would be different than for one surrounded by alkane moieties or other ester groups. Therefore, understanding the structure and energetics of diblock star polymers might imply a need for, at least, polarizable force fields.[21−26] However, the development and validation of these force fields is currently an evolving field, and their computational cost is still significantly greater than that of fixed charge force fields. Therefore, fixed charge force fields are still a good starting point for the study of these types of molecular systems, pending the availability, validation, and improved performance of more sophisticated treatments.

Since the use of fixed charge force fields raises questions about the quality of the balance of the intra- and intercomponent interactions among the three types of components of these systems (hydrophobic polymeric material, hydrophilic polymeric material, and water), this work examines the star polymer behavior as a function of the temperature. Behavior in the simulations that is seen to persist over a wide temperature range near physiological conditions is more likely to be predictive than behavior that is very sensitive to the

temperature near physiological conditions. Also, studying the temperature dependent behavior of the star polymer structure and kinetics will provide a point of comparison with similar changes in bulk polymeric material properties that occur at glass transition and melting temperatures.

This paper is structured as follows: Section 2 describes our methods, including a description of the ;molecular systems and the force fields and methods used to prepare, equilibrate, and simulate them; as well as the types of analyses performed to determine structural, thermodynamic, and kinetic properties. Section 3 presents results, and section 4 is a discussion of these results as well as predictions to be experimentally tested. Finally, section 5 presents general conclusions and also discusses further possible implications of this work for the design of diblock star polymers for drug delivery.

2. METHODS

a. Molecular Systems. Each of the star polymer systems was prepared by connecting 16 linear diblock copolymer arms to an adamantane junction. The carbon atoms of adamantane, $C_{10}H_{16}$, have a rigid 10 atom diamond-lattice structure (Figure 1). The 16 sites that are hydrogen atoms in adamantane were used as the connection sites for the hydrophobic part of each diblock arm. For each star system, the hydrophobic part of each arm was then connected to a short chain of six polyethylene oxide units. The first star polymeric system consisted of 16 arms each with 16 monomeric units of L-lactic acid (LA = $-C(HCH_3)-CO-O-$), a "linker" methylene unit ($-CH_2-$), then six units of ethylene oxide (EO = $-CH_2-O-CH_2-$), the last of which was terminated with a hydrogen atom to form a terminal methyl group. This system can also be described as $A[LA_{16}-CH_2-EO_6-H]_{16}$. The methylene group was included to link the PLA appropriately to the PEO. Each adamantane carbon is bonded to the stereocenter carbon of the first lactic acid unit in either one or two arms. This system will later be referred to as the polylactic acid (PLA) star polymer.

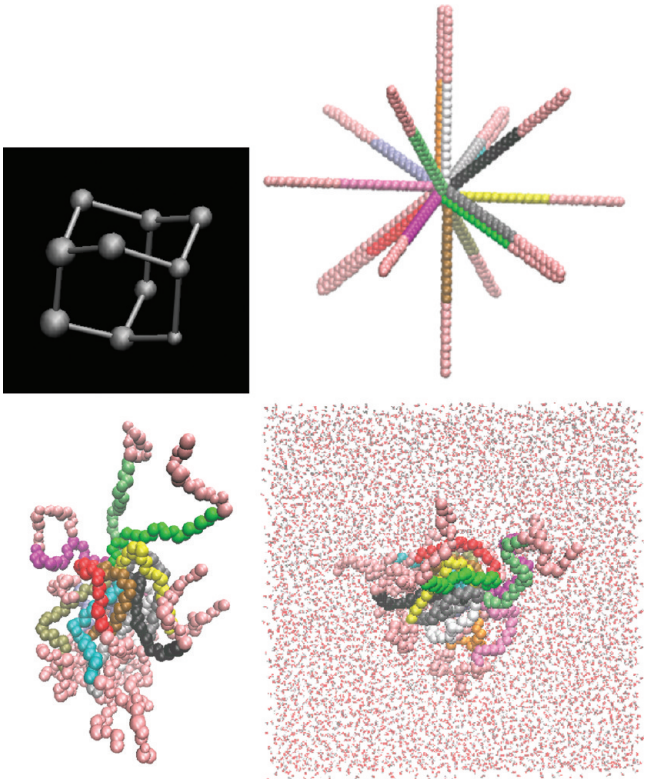

Figure 1. Schematic representations of star polymer construction for this study. Upper left: the adamantane junction showing the frame of 10 carbon atoms, four of which support the attachment of one arm and six of which support two arms. Upper right, a fully extended 16 arm star polymer with arms attached to the adamantane junction. Hydrophobic portions of the diblock arms are in different colors; the hydrophilic portions are all colored light brown. Lower left: representative "open" conformation produced after a small amount of simulation in the vacuum phase. Lower right: a solvated structure. These figures are not drawn to the same scale; see the text for relative sizes.

The second type of star polymer system was constructed using eight units of delta-valerolactone (VL = $-CH_2-CH_2-O-CO-CH_2-CH_2-$) for the hydrophobic part of the arm, followed, as before, by six units of ethylene oxide terminated with a methyl group. This system is described as $A[VL_8-EO_6-H]_{16}$ and will be referred to as the polyvalerolactone (PVL) star polymer.

The third type of star polymer system was constructed using 12 units of ethylene (E = $-CH_2-CH_2-$), an alkane chain of 24 carbon atoms, for the hydrophobic part of the arm, followed with six units of ethylene oxide terminated with a methyl group. This system is described as $A[E_{12}-EO_6-H]_{16}$ and will be referred to as the polyethylene (PE) star polymer.

As mentioned above, these systems are identical in composition except for the hydrophobic regions, and the variation was designed to span the range of polar vs nonpolar character, ester vs alkane content, and torsional flexibility. The lengths of the hydrophobic segments in each of the three star polymers were chosen to yield approximately equal arm lengths.

The molecular systems were built with arms in a fully extended state (Figure 1), and their length is noted in Table 1. The amount of this length due to the PEO part of each arm is approximately 21 Å.

Table 1. Summary of Star Polymer Systems Studied[a]

name	system	approx. extended arm length, Å	number atoms	number water	core volume
PLA	$A[LA_{16}-CH_2-EO_6-H]_{16}$	67	3050	45377	5860
PVL	$A[VL_8-EO_6-H]_{16}$	78	2618	45702	4650
PE	$A[E_{12}-EO_6-H]_{16}$	50	1850	46115	2432

[a]Core volume, in $Å^3$, is used to derive scaling factors that allow comparison among systems (see text).

b. Force Field. The force fields used for these simulations were mainly the OPLS-AA (all atom) force field[16] but with a number of exceptions. For adamantane, parameters similar to those for cyclohexane were used but with the improved parameters of Price et al.[17] for the alkane torsion angle energy expressions. For the linkage of the adamantane to the hydrophobic chains and for polyethylene segments, standard alkane parameters were used with the same improved torsion expressions. OPLS-AA parameters for esters (the polylactic acid and polyvalerolactone star polymers) were obtained from the same reference.[17]

Although most of the OPLS-AA force field parameters for esters were readily available, polylactic acid, an alpha-polyester, required some parameters that had not been published. These

dx.doi.org/10.1021/ct300188e | J. Chem. Theory Comput. 2012, 8, 3733−3749

relate to the torsional expressions for sites along the backbone of the PLA polymer. Parameters for the CT−C−OS−CT torsion exist,[17] but not for C−OS−CT−C or OS−CT−C−OS. (In OPLS-AA notation, C represents a carbonyl carbon; OS, an alkoxy oxygen in an ester; and CT, a generic alkane-like carbon.) For the missing torsional parameters, we substituted those for C−OS−CT−CT and CT−CT−C−OS torsions, respectively, since the middle bond in each case has the same character and multiplicity. Because of its commercial importance, recent efforts[27] have attempted to develop a better OPLS-like parameter set for polylactic acid simulations. These efforts have included extensive fitting to bulk properties of PLA, such as glass transition temperatures, and resulted in functional forms that are more complex than the ones used in this work. It is not clear whether such a potential would improve the model accuracy in the context of a star polymer in water.

Because of its importance for numerous applications ranging from use as a polymeric solvent in batteries to improving the solubility of pharmaceuticals, a considerable amount of effort[20,28−33] has been spent to develop and improve force field parameters for polyethylene oxide (PEO), also known as polyethylene glycol (PEG). These efforts usually start with quantum chemical studies of a simple commercially available dimer of ethylene oxide, 1,2-dimethoxyethane (DME), for which a great deal of reliable experimental data[34,35] exist that are useful for guiding and validating force field efforts. It has turned out to be particularly difficult for a force field model to yield the correct conformer populations for bulk liquid DME, available from the analysis of Raman spectra,[34] where the gauche conformation of the central O−C−C−O torsion appears to be unusually stable relative to, say, that of butane, a phenomenon known as the "gauche effect." The work of Anderson and Wilson[28] sought to produce a DME force field that improved upon both OPLS-AA and the potential of Smith et al.,[29,30] with respect to the these conformer populations. They employed higher quality quantum calculations than had been used in previous work to produce torsional energy maps for the three torsion angles involving the six heavy atoms of DME. Then, using the OPLS-AA charges and Lennard-Jones, bond, and angle parameters, they refitted only the C−C−O−C and O−C−C−O torsional parameters to best reproduce the quantum potential energy surface. This resulted in a substantial improvement in the conformer populations in bulk DME over previous implementations.

One of our concerns with the resulting Anderson−Wilson DME force field, however, was the possibility that it was insufficiently polarized to represent PEO in an *aqueous* environment. Earlier work[36,37] has shown that charges based on a solvent-polarized wave function can produce better solvation results. Using an approach very similar to that of Anderson and Wilson, we produced a potential for the star polymer simulations that we felt would represent the polarization of DME in water. Briefly, we generated an optimized structure for DME in the ttt conformation using an MP2 level of theory, but with a polarizable continuum[38] model (PCM) to represent an aqueous environment. The resulting charge density was used to evaluate the electrostatic potential (ESP) around the molecule, which was then fitted using point charges at the nuclear sites. After symmetrization, these charges were 0.003/0.068 for C/H of the terminal methyl groups, 0.142/0.049 for the C/H of the methylene group, and −0.447 for the oxygen. (The unit of charge is the electron.) This is in contrast to the charges 0.110/0.030, 0.140/0.030, and −0.400, respectively, used in OPLS-AA and in the Anderson−Wilson potential. Then, using these charges along with the OPLS-AA parameters for the bond and Lennard-Jones expressions, the C−C−O−C and the O−C−C−O torsional expressions were fitted to best reproduce a gas phase torsional energy map of a quality (MP2) similar to that used by Anderson and Wilson. The results are shown in Table 2, where

Table 2. Parameters for the Torsional Energy Expressions Involving Backbone Atoms in DME[a]

torsion	force field	V_1	V_2	V_3	V_4
O−C−C−O	DMEFF	2.8198	−2.5606	0.8216	−0.9203
C−O−C−C	DMEFF	1.6678	−0.5653	−0.0033	−0.2931
O−C−C−O	IBM	1.6224	−2.4022	0.2672	−0.1864
C−O−C−C	IBM	0.2770	−0.0086	0.2630	0.0178

[a]Values, in units of kcal/mol, are used in the expression $E(\phi) = (V_1/2)(1 + \cos(\phi)) + (V_2/2)(1 - \cos(2\phi)) + (V_3/2)(1 + \cos(3\phi)) + (V_4/2)(1 - \cos(4\phi))$. DMEFF refers to the work of Anderson and Wilson;[28] IBM refers to the current work.

one can see that the torsional fitting parameters are very sensitive to the charge model, even though in OPLS the 1−4 electrostatic interactions are scaled by a factor of 0.5. Conformational analysis using the resulting potential for liquid NpT simulations of bulk DME at 298 K and 1 atm is shown in Table 3, along with other published results. One can see that

Table 3. Populations of Conformers of DME in Bulk Liquid Given by Different Force Fields and by Experimental Results[a]

conformation	OPLS-AA	SJY	DMEFF	IBM	Raman
ttt	13.5	18	15.4	5	12
tgt	50.3	45	51	55	42
ttg	5.2	9	5.1	2	4
tgg	13	8	7.8	10	9
tgg′	14.6	17	18.4	24	33
ggg	1.4		0.4	1	
ggg′	1.4		1.2	2	
gg′g	0.1		0.3	0	
gtg	0.3		0.2	0	
gtg′	0.2		0.2	0	
Total	100	97	100	99	100

[a]OPLS-AA and DMEFF data are from Anderson and Wilson,[28] column labeled SJY is from Smith et al.,[31] and Raman data are from Goutev et al.[34]

the new model, polarized appropriately for solvation by water, still does fairly well at getting the conformer populations in bulk DME, slightly overpopulating the tgt conformer, underpopulating the tgg′ conformer (like the other force fields listed), and doing slightly worse with population of the less prevalent ttt conformer.

The charges actually used on the PEO segments of the star polymers were 0.142/0.049 for the methylene group and −0.48 for the oxygen, the final oxygen charge being more negative by 0.08 than used in OPLS-AA. Admittedly, the change in charge model relative to OPLS-AA is rather small. The improvement of conformer populations is quite likely due to the fitting of torsional energy parameters to high quality quantum chemical results. Further testing of this potential should be done to assess its applicability in other contexts.

The water model used was TIP4P-Ew, developed[39] as a variant of TIP4P,[40] and tuned for use in the context of Ewald treatments of the long-range electrostatic interactions. Since these data were used in the parametrization of the model, the TIP4P-Ew potential accurately reproduces pure liquid water density and heat of vaporization data over a broad temperature range. However, the model also reproduces structural properties such as the radial distribution function and kinetic properties such as the self-diffusion coefficient over a broad temperature range, and these were not used in the parametrization. In addition to being developed for use in the context of Ewald methods, the fitting of the TIP4P-Ew parameters to experimental heat of vaporization data took account of the difference in energy between an unpolarized gas phase water molecule and one polarized to the extent implied by the fixed charges of the model, also known as the electronic polarization cost. Consideration of polarization cost in the fitting was also done in the development of TIP4P/2005,[41] but it was *not* done in the development of TIP4P.[40] Treating the polarization cost has led to substantial improvement in the accuracy of the structural, thermodynamic, and kinetic properties of both of these models.[39,41]

c. Simulations. Structural models were prepared for all three star polymer molecules using locally developed software. The models are simply the atomic Cartesian coordinates for each atomic site of the molecules constructed with each polymeric arm in a fully extended state (see Figure 1). These molecular structures have end-to-end distances as large as 160 Å (see Table 1). Force field parameters were assigned, also using locally developed software, and input files were prepared for the LAMMPS simulation package.[42] Short structural optimizations were performed followed by short simulations on these molecules without solvent, i.e., in the "gas phase", during which the molecules were allowed to partially collapse into more compact but still somewhat open structures. These partially collapsed structures (see Figure 1) had end-to-end distances ranging from 48 Å (PVL) to 58 Å (PLA).

A cubic simulation cell of 46 656 TIP4P-Ew water molecules was prepared and equilibrated using locally developed software and a protocol previously described[39] with a control temperature of 300 K and an external pressure of 1 atm. A set of particle coordinates was obtained from the resulting simulation (cell edge length 111.9453 Å) representing an instantaneous density of 0.9949 g/cm^3, in excellent agreement with experimental values. (At a temperature of 298 K and a pressure of 1 atm, the mean density of water using the TIP4P-Ew water model[39] is 0.9954 g/cm^3; the corresponding experimental value is 0.99716 g/cm^3.)

The starting conformation for the simulations of solvated star polymers was made as follows: (1) The coordinates of the star polymer sites were translated so that the center of geometry was at the center of the cubic simulation cell from the water equilibration simulation. (2) For each water molecule, the smallest distance from any of its three sites to any of the sites on the star polymer was computed. (3) Using these distances, water molecules were removed from the simulation, starting with the one closest to the star polymer and then the one next closest and so on, until the total mass of removed water molecules first exceeded the total mass of the star polymer. Between 541 (PE) and 1279 (PLA) water molecules were removed by this procedure. This process produced a set of three systems, one for each star polymer. By construction, each of these had the same volume and very nearly the same mass, and hence the same mass density, as that of water. With the closest water molecules removed in this way, dynamical simulations could be started without any additional preparation (see Figure 1).

Most of the production simulations were performed using a version of the LAMMPS software[42] dated July 7, 2009. The LAMMPS software performs and scales well on massively parallel computers for molecular systems of the size and type studied here. Molecular dynamics simulations were performed on an IBM BlueGene/L supercomputer, and most of the analysis of the resulting trajectory data was performed on a cluster of IBM AIX workstations.

All equilibration and production simulations were performed using the NVT ensemble, with thermal control implemented in LAMMPS using a Nose−Hoover extended Lagrangian procedure, with a fictitious mass set so as to establish a fluctuation period[43] of approximately 100 fs in the thermostat variable, known as the thermostat damping factor in LAMMPS. The dynamical integration scheme was velocity-Verlet[44] with a time step size of 1 fs. All bond lengths involving hydrogen, as well as the HOH angle for the TIP4P-Ew water, were constrained using a SHAKE procedure[45] to guarantee that bond length constraints were satisfied to a tolerance of 10^{-5} Å. Lennard-Jones interactions and direct space electrostatic interactions were truncated at 9 Å. A tail correction for the part of the Lennard-Jones potential beyond this cutoff was included in the energy and pressure computation. Electrostatic interactions were evaluated with a particle−particle−particle mesh (PPPM) procedure[46] with an accuracy parameter (10^{-5}) that resulted in a 3D grid of 120-by-120-by-120. In accordance with the OPLS-AA potential, neither Coulomb nor Lennard-Jones interactions are evaluated for particle pairs that are 1−2 and 1−3 interactions, and both of these types of interactions are scaled by a factor of 0.5 for 1−4 interactions. Geometric combining rules were used to establish the Lennard-Jones parameters.

Thermal equilibration was performed for each of these systems at four different temperatures: 300, 350, 400, and 450 K. Some of these equilibration simulations were as long as 50 ns. During the thermal equilibration phase for each solvated star polymer system, the star polymer molecules collapsed slightly more, and for each system, the edge length of the simulation cell was greater than twice the linear dimension of the star polymer molecule. Under the minimum image convention, this guarantees that the closest image of each site in the star polymer to any other site is from the same image, thereby preventing the apparent direct interaction between copies of the star polymer molecule in different periodic images. Production runs for these three solvated molecular systems at the four temperatures were at least 20 ns.

d. Analysis. During the production phase of the simulations, solute and solvent coordinates were saved to disk for analysis at intervals of 10 ps, resulting in at least 2000 sets of coordinates for each of the three molecules and at each of the four temperatures. Since in most cases these represented highly correlated data, detailed analysis was performed only on one-fourth of this data, on coordinates spaced at intervals of 40 ps. The analysis consisted of the calculation of several structural observables as well as a Voronoi analysis. The structural observables included such things as maximum end-to-end distance, spherically averaged mass density, and molecular shape descriptors[47] derived from the eigenvalues of the gyration tensor such as the radius of gyration, asphericity, and

anisotropy.[48] In order to characterize the intramolecular chain structure and dynamics without the effect of overall star polymer molecular rotation, a molecule-centered reference frame was defined with an origin and orientation determined by the coordinates of the sites of the relatively rigid adamantane core. For each coordinate set, the atomic site coordinates as well as the coordinates of an orientational unit vector associated with each monomeric unit of the star polymer were measured with respect to the molecule-centered reference frame.

Voronoi analyses were also performed for each set of coordinates. A Voronoi analysis[49,50] constructs a set of polyhedra, one polyhedron around each atomic site of the system (all water sites plus all star polymer sites). These polyhedra collectively fill all space of the simulation cell, and each one encloses a volume of space that is closer to its associated site than to any other site. Voronoi polyhedra faces that are shared by two polyhedra, consist of points that are equidistant to the two sites associated with the polyhedra. Similarly, points on a polyhedron edge are equidistant to three such sites, and each polyhedron vertex is equidistant to four. Voronoi analysis uses only the Cartesian coordinates of the atomic sites in the simulation, without any knowledge of the molecular identity, chemical nature, or bond connectivity of the material. However, all of this information manifests itself in the Voronoi analysis through the resulting distribution in the number of faces, the facial shapes and areas, polyhedral volumes, etc. For our purposes, we partitioned the sites into different classes and used the Voronoi polyhedra associated with each class to compute a volume for the class, and the interfacial surface area shared between pairs of classes. The interface between two classes consists of the union of all Voronoi faces that are shared by two polyhedra where one polyhedron is associated with one class and the other polyhedron is associated with the other class. For example, by establishing three classes that we associate with "water", "hydrophobic", and "hydrophilic" sites, we can compute the total volume occupied by each class and the interfacial surface area between the hydrophobic and hydrophilic material, as well as between the water and the hydrophilic material. This technique provides a more general alternative to the solvent accessible surface area metric[51] that is often used.

An important issue for the use of star polymeric materials for drug delivery relates to the amount of water in the interior of the polymer, specifically the hydrophobic region. Water content potentially affects the release rate of the drug as well as the rate and mode of degradation of the polymer itself. Important metrics therefore include the thermal and compositional dependence of the amount of water, its penetration depth, its diffusion within the star polymer, and the exchange rate of water into and out of (e.g., water lifetime) the hydrophobic regions. The difficulties of measuring this in simulations begins with how one should define what molecules are actually in the hydrophobic region, since there is really not a well-defined interface between components when examined at a molecular level.

The issue of water penetration was explored also using Voronoi analysis, since it provides a useful way of determining if two molecules are neighbors: two sites are Voronoi "neighbors" if their Voronoi polyheda share a face. A cluster analysis was performed on the water molecule sites in each coordinate set using the neighbor list developed by the Voronoi analysis. Two water sites were defined as being in the same water cluster if they were Voronoi neighbors. This clustering procedure partitions the water molecules into one or more sets, each of which is a "contiguous" water cluster, with the largest, of course, representing the bulk solvent. Other clusters of water molecules, if they exist, are, by construction, not neighbors of any of the bulk water molecules and, so, are surrounded only by star polymer sites. We designate such clusters as "interior" clusters as distinguished from the "bulk" cluster. With this approach, information can be collected about the number, size, and shape distribution of such interior water clusters, the nature of their environment (e.g., the amount of the water cluster's surface area that is in contact with hydrophobic vs hydrophilic regions of the star polymer), and their evolution and lifetime within the star polymer. By computing the closest distance from each oxygen site in an interior water molecule to the oxygen sites in the bulk water, one can get a sense of the penetration "depth" into the star polymer of the interior absorbed water.

In general and at most sampling rates, observables computed from molecular dynamics simulation data are highly correlated. In several instances where statistical uncertainty is reported, correlation in the data was taken into account by computing the fluctuation autocorrelation function for the observable of interest. The correlation time was taken as the area under this function. Since this function itself is subject to uncertainty and becomes more noisy with greater lag times, it is integrated only up to the point where it first goes negative, giving an estimate of the correlation time, τ_c. The uncertainty (standard deviation of the mean) in an observable is then given as the root-mean-square deviation in that observable times the square root of $2\tau_c/T$, where T is the simulation time over which the observable is averaged. ($T/2\tau_c$ is the effective number of uncorrelated samples.) There is always some danger in computing such correlation times and resulting uncertainty estimates, since for insufficiently long simulations the true magnitude and temporal variation of fluctuations of a signal are not observed, and hence, both the standard deviation and the correlation time are underestimated, resulting in an artificially small uncertainty which makes the result appear to be more statistically significant than it really is. Uncertainties in the numbers of rare events observed, such as instances of water penetrating into the hydrophobic regions of the star polymers, were assumed to be the square root of the number of observations, assuming these are governed by Poisson statistics.

3. RESULTS

Renderings of representative configurations of the three molecular systems at the lowest (300 K) and highest (450 K) temperatures studied are shown in Figures 2−4. For the PLA and PVL molecules, the images do not convey much difference between the high and low temperature, nor even between the PLA and PVL star polymers. The PE system, on the other hand, shows a considerable amount of ordered structure, even at high temperatures. Animated models (videos) of these molecules suggest that the PEO regions are very mobile, but the hydrophobic regions are very rigid (crystalline or glassy) on the 20 ns time scale of these simulations.

Radius of gyration (R_g) data are shown in Figure 5. For each molecule and at each temperature, the average radius of gyration was computed using the entire star polymer (filled symbols and solid lines) as well as without consideration of the hydrophilic part, in order to characterize the spatial extent of the hydrophobic core. From the figure, one can see that there is very little temperature dependence except for the PE system,

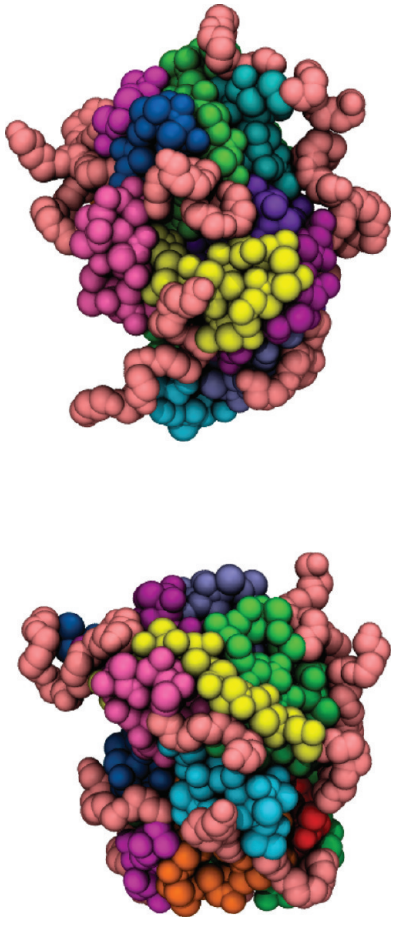

Figure 2. Renderings of representative configurations of the PLA star polymer at 300 K (top) and at 450 K (bottom). The hydrophobic region of each of the 16 arms is shown in a different color. The hydrophilic (PEO) terminal region of each arm is colored light brown.

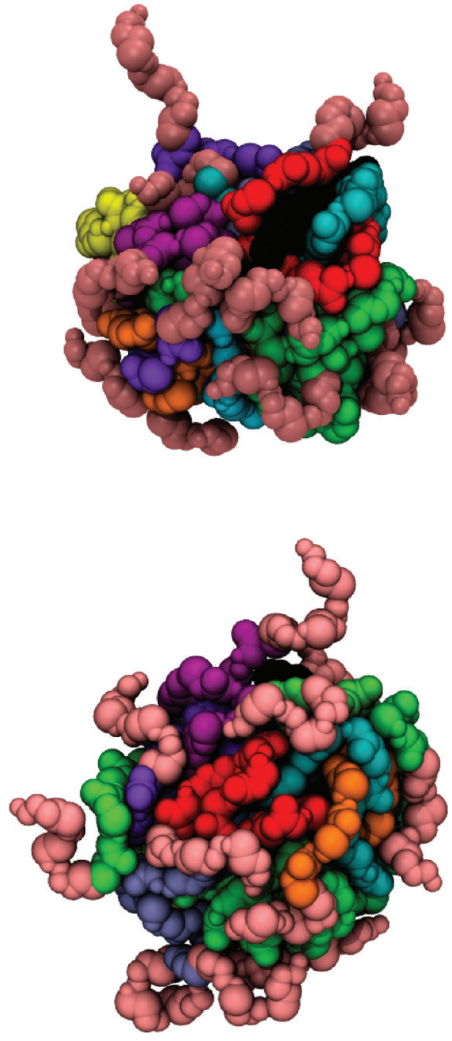

Figure 3. Renderings of representative configurations of the PVL star polymer at 300 K (top) and at 450 K (bottom), colored as in Figure 2.

which shows a significant drop in R_g between 350 K and 400 K, suggesting a transition to a more compact state. Figure 6 shows the thermal dependence of the magnitude of the fluctuations in R_g. The general increase with temperature indicates a gradual increase in the compressibility. It is notable that even though there is a discontinuous change in R_g for the PE star, there is no such behavior in the magnitude of the fluctuation in this quantity. Figure 7 shows the thermal dependence of the anisotropy. This dimensionless metric can range from zero (spherical) to unity (long rods). The change in anisotropy for the PE star on going from 350 K to 400 K indicates a change from an elongated to a more spherical shape.

The behavior of some of these star polymers at the lowest temperature shows some anomaly in R_g (PLA), its fluctuation (PVL and the hydrophobic core of PLA), and the anisotropy (PLA). This may be an indication that at 300 K the relaxation times and correlation times may be so long for PLA and PVL that thorough sampling is difficult to achieve over the 20 ns period of the production simulations. Other observables suggest this as well. The uncertainty estimates are larger at these temperatures but might still be underestimated.

The spherically averaged mass density at 350 K, as a function of the distance from the center of mass of the adamantane, is shown for the three molecules in Figures 8−10. These figures illustrate the contribution to the total mass density from various components: adamantane, the hydrophobic material, the hydrophilic material, and water. These figures indicate that close to the adamantane the material is highly structured. In fact, having 16 polymeric arms attached to an adamantane core produces a significant amount of local strain in the model that persists along each arm until the density decreases enough for more favorable and random chain conformations to be adopted. These graphs show very little thermal dependence (data not shown for other temperatures), except for a gradual smearing of some of the features of the hydrophobic material. One can see that the hydrophilic material adopts a broad featureless distribution in each case. The figures also appear to suggest that there are rather diffuse boundaries between materials, with considerable interpenetration of water and hydrophilic material into the hydrophobic material. However, further analysis indicates this is an illusion created by the spherical averaging process when the hydrophobic core is highly nonspherical (PE) or has a rough surface with many grooves and valleys (PLA and PVL) that allow water to get relatively close to the adamantane core without actually penetrating into the hydrophobic core material itself.

The mass density plot for the PE polymer (Figure 10) exhibits a feature not seen in the other two polymers: there is a more slowly decaying curve for the hydrophobic material. Whereas the mass density due to hydrophobic material falls

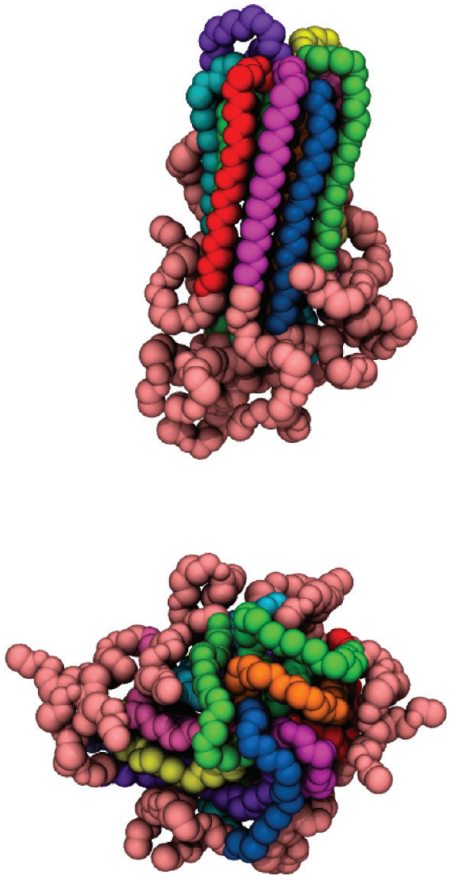

Figure 4. Renderings of representative configurations of the PE star polymer at 300 K (top) and at 450 K (bottom), colored as in Figure 2.

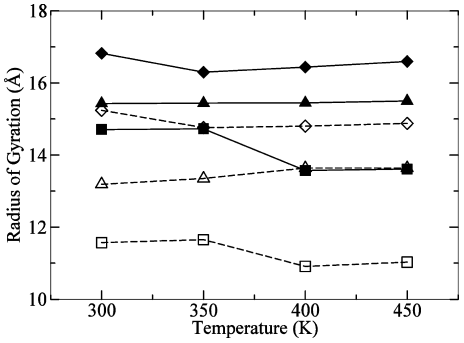

Figure 5. Radius of gyration, computed from the gyration tensor, for each star polymer at each of four temperatures. Symbols represent PLA (diamonds), PVL (triangles), and PE (squares). Solid symbols and solid lines represent the radius of gyration for the entire star polymer; open symbols and dashed lines represent that of just the hydrophobic material. Uncertainty estimates, ±2 standard deviations, are not shown but are approximately the size of the symbols, usually 0.1 Å or less.

from 0.5 g/cm^3 to 0.1 g/cm^3 over a distance of 2.9 Å for the PLA and 3.2 Å for the PVL, this decrease occurs over a distance of 6.4 Å for the PE polymer. This is a manifestation of the crystalline and cylindrical nature of this polymer at 350 K, as indicated visually (Figure 4) and through other structural observables.

The structure in the mass density graphs can be resolved by a monomeric unit, and this is shown for PLA at 350 K in Figure 11. The first monomeric units of LA along each of the 16 arms

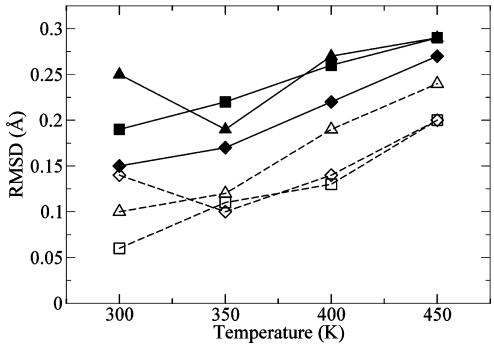

Figure 6. Root mean square deviation in R_g. Symbol and line type notation is the same as in Figure 5.

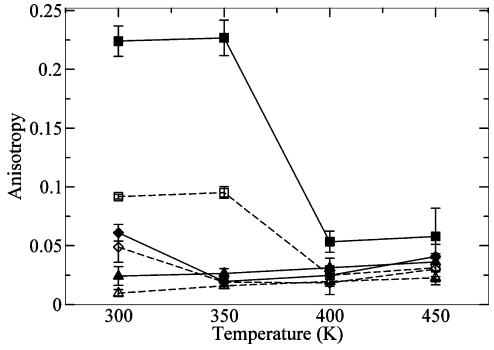

Figure 7. Anisotropy. Uncertainty estimates are ±2 standard deviations.

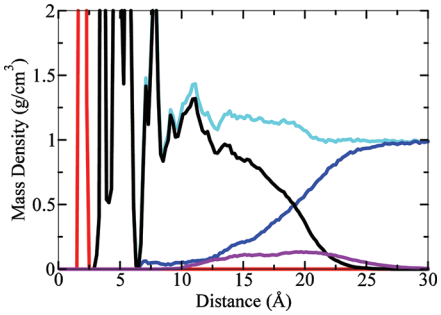

Figure 8. Orientationally averaged mass density for the PLA star polymer at 350 K as a function of the distance from the center of mass of the adamantane. The curves represent contributions to the total mass density (cyan) from the adamantane (red), from the hydrophobic material (black), from the hydrophilic PEO (purple), and from water (blue).

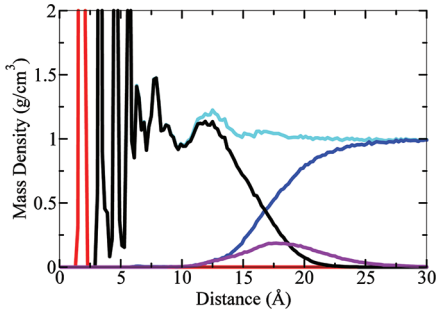

Figure 9. Orientationally averaged mass density for the PVL star polymer at 350 K. Coloring scheme is the same as for Figure 8.

dx.doi.org/10.1021/ct300188e | J. Chem. Theory Comput. 2012, 8, 3733−3749

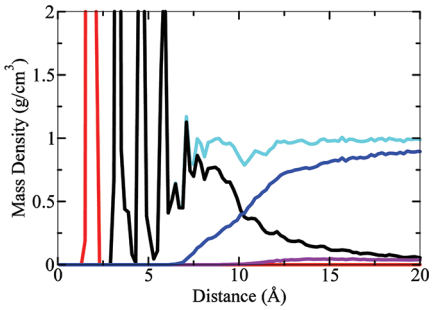

Figure 10. Orientationally averaged mass density for the PE star polymer at 350 K. Coloring scheme is the same as for Figure 8. In comparing this figure with Figures 8 and 9, one should note that the range of the *x* axis is different.

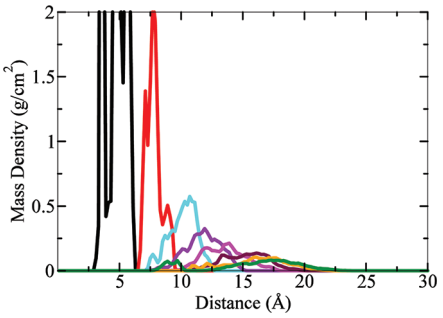

Figure 11. Orientationally averaged mass density contribution from hydrophobic material in the PLA star polymer at 350 K resolved by a contribution from different monomeric units. Each color corresponds to the mass density contributed by a different set of 16 lactic acid monomer units that are all at the same position along the arm as measured from the adamantane connection. The black curve represents mass density from the 16 lactic acid units that are directly connected to the adamantane.

produce three peaks in this graph (black) near a distance of about 5 Å; the second units of LA along the 16 arms produce peaks near 7 Å (red), and so on. As one moves out along the chains, the distributions become less structured and broader. Using this graph, one can determine which sets of monomeric units are responsible for the peaks in the total mass density. For example, the peak at 10.7 Å in black in Figure 8 (PLA) is due to the positioning of the third LA units along the arms (blue in Figure 11). The one at 11.7 is due to the fourth (purple) and fifth (magenta), and the soft peak at 13.3 is due to the fifth (magneta) and sixth. LA units farther than the fourth or fifth, and out to the last (16th), are behaving similarly and probably produce a density and chain packing at distances larger than about 12.5 Å that is more representative of what might be seen in even larger star polymers. In fact, even the fourth unit (purple) contributes significant mass density at distances closer to the adamantane than the third (blue), suggesting an ability to pack more closely. The fourth and fifth units along the chains are, therefore, "transitional" between the highly structured and more random units. Similar analysis identifies the transitional hydrophobic units for the other star polymers as the second for PVL and the third and fourth for PE. (The PVL units are much larger and floppier than the PLA and PE units.)

Orientational autocorrelation functions for selected individual repeat units for each star polymer at 350 K are shown in Figure 12. These were computed as follows. First, a local orientational unit vector (**u**) was defined for each monomeric

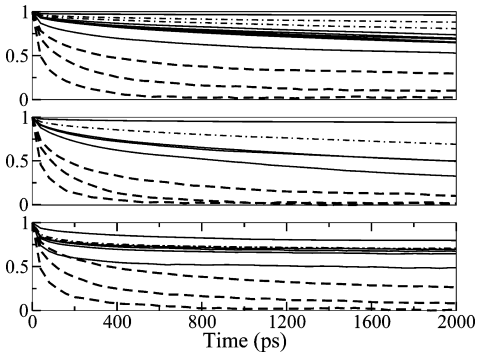

Figure 12. Orientational autocorrelation functions for monomeric units at 350 K for PLA (top), PVL (middle), and PE (bottom) star polymers. Each curve represents an average of the 16 autocorrelation functions that correspond to monomeric units at the same distance along each arm. Dot-dashed lines correspond to the "transitional" repeat units near the adamantane within the hydrophobic material. Solid lines correspond to various other hydrophobic monomeric units. Dashed lines correspond to hydrophilic PEO units. Correlation functions decay more and more quickly as one moves farther out along each chain away from the adamantane. For PLA (top), the lines refer to repeat units 2, 4*, 5*, 6, 8, 10, 12, 14, and 16. For PVL (middle), the lines refer to repeat units 1, 2*, 4, 6, and 8. For PE (bottom), the lines refer to repeat units 2, 3*, 4*, 6, 8, 10, and 12. Asterisks indicate the repeat units determined to be transitional.

unit on each arm of each star polymer. These vectors were directed between specific pairs of atomic sites on each monomeric unit. For the PLA and PVL, the vectors were directed between an alkoxy oxygen site and the first carbon site immediately opposite the nearest carbonyl group. For PE and PEO, the vectors were directed between pairs of adjacent (bonded) carbon sites. (Only three vectors were selected within the six unit PEO part of the chain.) Second, for each saved set of coordinates, these vectors were measured and projected from the lab frame onto the molecule-centered reference frame. Third, the time evolution of these vectors in the molecule frame was determined at 40 ps resolution over the 20 ns of the production simulations, and then an autocorrelation function ($\langle \mathbf{u}(0)\cdot\mathbf{u}(t)\rangle$) was computed for each monomeric unit. Next, groups of 16 of these functions that correspond to monomeric units at the same position along the star polymer arms were averaged. There is, therefore, a set of curves (19 for PLA, 11 for PVL, and 15 for PE) for each star polymer that shows different rates of decay, corresponding to the rate of loss of orientational memory for monomer units at various positions along each arm. Curves that correspond to monomeric units close to the adamantane do not decay at all, and the curves that correspond to the most distant PEO group decay very rapidly. (In Figure 12, approximately half of these curves are shown.)

The curves in Figure 12 illustrate several interesting points. First, the rate of decay in the correlation functions is nearly monotonic as one moves along each chain from the units closest to the adamantane outward. Second, for each molecule, there is a group of very slowly decaying curves that include the transitional units (identified above, and shown in Figure 12 with dot-dashed lines), and then a band of decaying curves that are closely spaced and sometimes overlapping that correspond to a more homogeneous temporal behavior of hydrophobic material outside of this transitional region. Third, there are one or two units in the hydrophobic region nearest the PEO that

dx.doi.org/10.1021/ct300188e | J. Chem. Theory Comput. 2012, 8, 3733−3749

have much faster decay than these, presumably because they are being "pulled" about by the more rapidly reorienting and solvated PEO units. Finally, the PEO units (dashed lines in Figure 12) have the fastest decay of orientational correlation, with the slowest one of those corresponding to the ones "tethered" to the hydrophobic units. These time correlation functions were computed at each of the four temperatures (not shown), and all graphs share these general features but with correlation times getting shorter with increasing temperature.

The curves in Figure 12 also indicate that at 350 K the hydrophobic material is not reorienting on a 2 ns time scale for the PLA and PE, and the PVL core is behaving only slightly more fluid-like, suggesting these cores are more like a solid (crystalline for PE, disordered and glassy for PLA and PVL) than a liquid. In fact, the middle band of PE correlation times (bottom of Figure 12) shows no decay at all, and the structure appears to be rigid and crystalline (Figure 4). Even though they do not decay much on a 2 ns time scale, the hydrophobic PVL correlation functions show faster decay than those of either PLA or PE, indicating that PVL could be somewhat more fluid-like than either the PLA or the PE polymers. This may be due to the alkane regions of the hydrophobic segments offering more flexibility than what is available in the PLA, and the ester regions preventing the chain registration and alignment of the alkane segments that is seen to stabilize the crystalline structures of the PE.

The Voronoi analysis was performed on coordinate sets at a 40 ps temporal resolution, and interfacial surface areas between water, hydrophobic, and hydrophilic materials were measured and averaged for each star polymer at each temperature. Figure 13 shows the interfacial area exposed by the hydrophobic

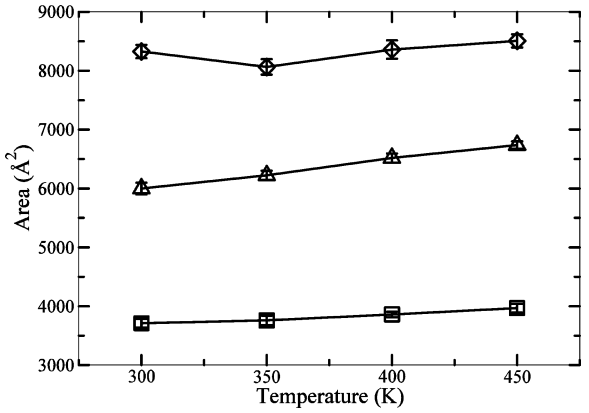

Figure 13. Total interfacial area of hydrophobic material (sum of hydrophobic–hydrophilic and hydrophobic–water interfacial areas) for the PLA (diamond), PVL (triangle), and PE (square) star polymers. Uncertainty estimates are ±2 standard deviations.

material, which is the sum of the hydrophobic–water and hydrophobic–hydrophilic interfacial areas. Except for the PLA star at 300 K, which might be exhibiting insufficient sampling as discussed above, these show a gradual increase with the temperature probably related to the swelling seen in the fluctuations of the radius of gyration. Figure 14 shows the part of this that is due to the interface between the hydrophobic material and water. These generally show an increase with the temperature, except for PLA at 300 K, and a noticeable drop between 350 K and 400 K for the PE star, where it changed from an elongated structure to a more globular one. It would make sense for some aspect of the PE star hydrophobic surface

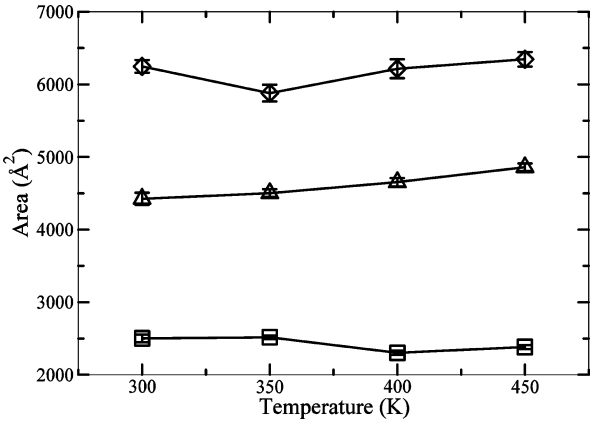

Figure 14. Interfacial area between hydrophobic material and water for the PLA (diamond), PVL (triangle), and PE (square) star polymers. Uncertainty estimates are ±2 standard deviations.

area to change during this structural change. A decrease in the hydrophobic contact area with water (shown in Figure 14) makes sense, but the fact that the total surface area (Figure 13) did not change very much indicates that that the hydrophilic–hydrophobic interfacial area increased to compensate. Images of the PE star (Figure 4) suggest why this happened. The elongated cylindrical PE structures seen at low temperatures are very crystalline, organized into a cylindrical shape with all of the PEO at one end. At higher temperatures where this structure gives way to a more globular shape, there is more opportunity for the hydrophilic PEO parts of the chains to come into contact with the hydrophobic parts, thereby simultaneously decreasing the water contact (Figure 14) and increasing the PEO contact (Figure 16) after the collapse. The trend in

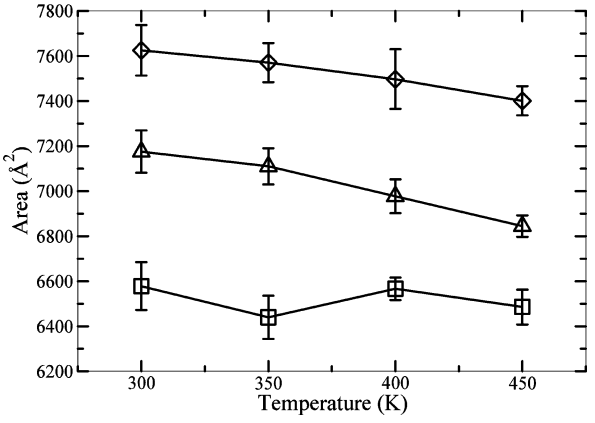

Figure 15. Total interfacial area of PEO hydrophilic material (sum of hydrophobic–hydrophilic and hydrophilic–water interfacial areas) for the PLA (diamond), PVL (triangle), and PE (square) star polymers. Uncertainty estimates are ±2 standard deviations.

hydrophobic surface areas seen in Figures 13 and 14, PLA > PVL > PE at all temperatures, is simply a reflection of the fact that these star polymers are of somewhat different sizes, simply because of the number and size of the repeat units in their hydrophobic regions (see Table 1).

Figure 15 shows the total PEO interfacial area, which is the sum of the contact area with water and with the hydrophobic material. The increase in PEO total surface area for the PE star on going from 350 to 400 K can be understood as the dense

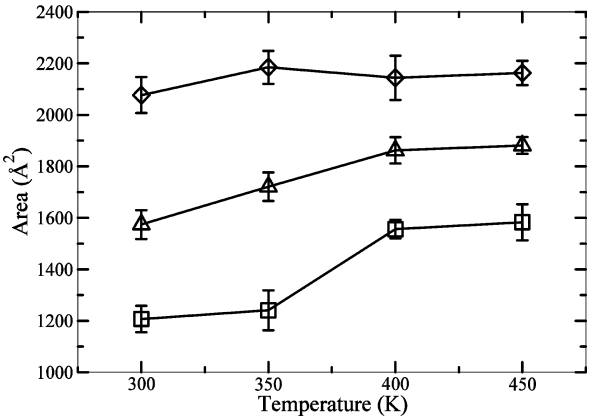

Figure 16. Interfacial area between hydrophilic (PEO) and hydrophobic material for the PLA (diamond), PVL (triangle), and PE (square) star polymers. Uncertainty estimates are ±2 standard deviations.

PEO structure at the end of the cylindrical structures seen at low temperatures (Figure 4) is broken up at higher temperatures, allowing more PEO to be exposed to water and to the hydrophobic PE in these more globular conformations. However, other features of Figure 15 are rather surprising in that there is a general and significant decrease in PEO surface area with increasing temperature for each polymer, even for the PE on each side of the transition. This decrease suggests that PEO may be aggregating with itself, decreasing contact with water and perhaps with hydrophobic material, and that this is somehow more pronounced at higher temperatures.

Figures 16 and 17 show the PEO–hydrophobic and PEO–water interfacial areas, respectively. Contact between PEO and

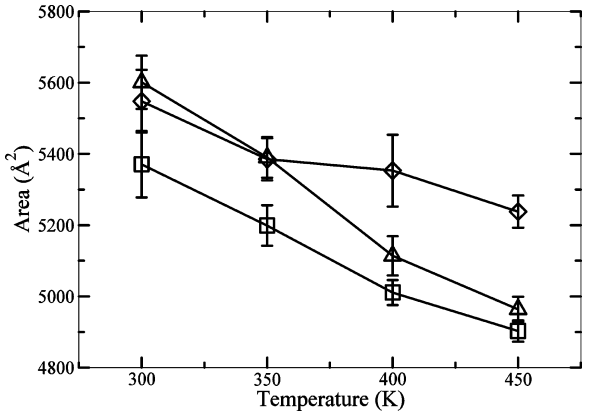

Figure 17. Interfacial area between hydrophilic (PEO) material and water for the PLA (diamond), PVL (triangle), and PE (square) star polymers. Uncertainty estimates are ±2 standard deviations.

hydrophobic material actually *increases* or is relatively flat with the temperature, but the contact with water decreases by even more, indicating a preference for PEO to attempt to "phase separate" from water at higher temperatures. This rather surprising observation may be consistent with the fact that PEO–water mixtures exhibit a lower critical solution temperature[52] (LCST) wherein a PEO–water mixture can change from a single phase (miscibility) to a two phase system with increasing temperature. The possibility of this phenomenon being exhibited in star polymers, where it might be tunable by modifications of the chain length, the number of chains, or the chemical nature and size of the hydrophobic region, is worthy of further experimental and theoretical investigation. Figures 16 and 17 indicate that this tendency of PEO to self-associate is in competition with its tendency to associate with the hydrophobic material.

Also apparent from Figure 16 is the decrease at all temperatures in the tendency of PEO to cover the hydrophobic core as one goes from an ester-rich hydrophobic material (PLA) to a pure alkane hydrophobic material (PE), with PVL in between. Recall that the length of the PEO region of each arm is the same across all three polymers, so differences between PLA, PVL, and PE star polymers in the PEO interfacial areas with water and with hydrophobic material seen in Figures 15–17 are not due simply to differences in the sizes of the hydrophobic regions as is the case in Figures 13 and 14. Finally, regarding the numerical values of the PEO–hydrophobic interfacial surface areas in Figure 16, it should be recognized that these include the areas from the region of connection where the PEO segment of each arm connects to the hydrophobic segment of that arm. The contribution from these junctions varies considerably with chain orientation, but 35 Å^2 is a reasonable approximation, suggesting that there is about 560 (16 × 35) Å^2 of the interfacial PEO–hydrophobic area that should not be considered to be in contact in the usual sense of a PEO chain laying against the hydrophobic material. With this subtracted from each of the values in Figure 16, and the result compared with the values in Figure 17, one sees that there is about 2.5 times more contact between PEO and water than between PEO and the hydrophobic region of the PLA star. For the PVL star polymer, this factor is about 3, and for the PE star, it goes from over 4 at low temperatures to about 3 at high temperatures.

Apparent from a comparison of Figures 13 and 14 is that hydrophobic cores in these models are exposed to a great deal of water. From 60% to 75% of the hydrophobic surface area is in contact with water, and this increases to 70% to 80% if account is made for the approximately 560 Å^2 of junction regions that cannot be solvated. This may be due to the fact that the PEO regions of the chains are relatively short with only six PEO units. However, from comparison of Figures 15–17, as discussed above, one can see that given the choice between contact with water or with hydrophobic material, the PEO in our model has an overwhelming preference for water contact. A study of individual conformations reveals that the maximum contact area between one of the PEO segments and the hydrophobic region is approximately 234 Å^2, including the junction region. Therefore, a hypothetical fully coated hydrophobic region would produce about 3744 (16 × 234) Å^2 of PEO–hydrophobic interfacial area with PEO segments of the length studied here. Figure 16 shows significantly less than this at all temperatures and for all molecules. Similarly, the maximum interfacial area between an extended PEO segment and water is approximately 450 Å^2. So, if all PEO segments were maximally solvated, the aggregate PEO–water interfacial area would be approximately 7200 Å^2. Figure 17 shows that for each molecule and at all temperatures, the PEO–water interfacial area is a significant fraction of this "available" 7200 Å^2. And some of the deficit can be explained by PEO–PEO contact, including interchain contacts and intrachain contacts observed when a PEO segment adopts hairpin and coil conformations.

Voronoi analysis allowed for the identification of water clusters that permeated into the interior of the star polymers.

The average number of interior water molecules per configuration for each star and at each temperature is shown in Figure 18. Water penetration generally increases with the

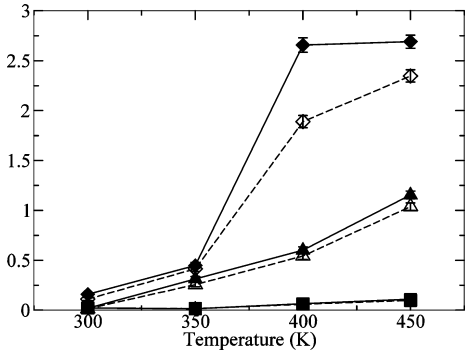

Figure 18. Average number of interior water molecules and water molecule clusters per configuration in the PLA (diamond), PVL (triangle), and PE (square) star polymers. Number of molecules is indicated with the solid lines and filled symbols; number of clusters is indicated with dashed lines and open symbols. Uncertainty estimates are ±1 standard deviation.

temperature but for the PLA showed a very large increase (almost 6-fold) on going from 350 K to 400 K. PLA is the most ester-rich of the star polymers studied, and this might explain its increased tendency to absorb water. However, even for this polymer and at the highest temperatures, there are only about 2.5 water molecules in a typical star polymer, so water penetration is rather rare.

The trend in the amount of interior water shown in Figure 18, PLA > PVL > PE, could be due to differences in the water accessible volumes of these star polymers, given that these polymers are of different sizes (see Table 1). To account for this, we normalized the values of Figure 18 by the water accessible volume for each star polymer. The Voronoi volumes of the hydrophobic regions of each star polymer were observed to be relatively temperature independent (24 400 Å^3 for the PLA star; 19 200 for the PVL; 10 400 for the PE). This volume includes the adamantane component and all of the hydrophobic material of each star polymer. However, the deepest part of this volume, consisting of the adamantane and the first few hydrophobic repeat units of each arm, are inaccessible to water due to the high density and steric crowding. Therefore, the volume of hydrophobic material accessible to water in each case is the total hydrophobic volume, minus a "core volume" (see Table 1) that includes the adamantane and the first hydrophobic repeat units of each arm out to the "transitional" units discussed earlier. The core volume includes adamantane plus the first four lactic acid units in the PLA star polymer, the first two valerolactone units of the PVL star, and the first three ethylene units (six carbons) of the PE star. Scaling the water content data of each star polymer in Figure 18 by the water accessible volume to account for these size differences does not significantly change the trend but makes the PLA and PVL appear a bit more similar, so that the water concentration follows the trend PLA ∼ PVL > PE. An alternative to this, normalizing the water content by the total hydrophobic surface area, produced similar results.

For each interior water molecule, its depth "into" the polymer was computed as the distance from the oxygen site of that interior water to the closest oxygen of a water molecule in the bulk. By our definition of an interior water molecule, there must be at least one intervening Voronoi polyhedron from a star polymer site separating these oxygen sites, so there is a minimum bulk to interior water distance observed of about 4 Å by this metric. These depth profiles are shown in Figure 19 for

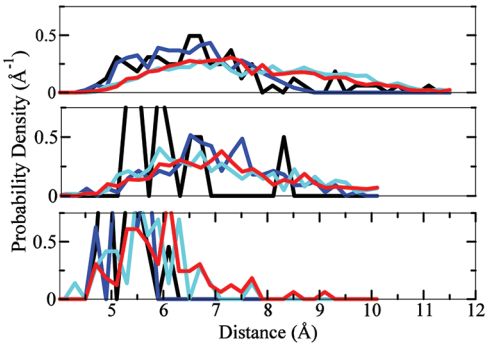

Figure 19. Depth profiles for water molecules penetrating into the interior of star polymers. Top panel is for PLA, middle for PVL, and bottom for PE star polymers. In each case, the lines represent the probability density by depth for 300 K (black), 350 K (blue), 400 K (cyan), and 450 K (red).

each star polymer at the four temperatures studied. It can be seen that these curves are very noisy at low temperatures since so few interior water molecules were observed (<0.5 per frame). As the temperature increases, the curves get smoother and penetration is deeper into the interiors of the star polymers. The penetration depth follows the trend PLA > PVL > PE, suggesting again that ester-rich environments may be somewhat more favorable to water than alkane environments. However, one must also keep in mind that the sizes of these star polymers differ, and some of the penetration depth trend could be explained by that.

The number and duration of water penetration events were also noted. We defined a water penetration "event" as having a beginning time, the time of first observation of the water molecule in the interior (immediately before which it was not in the interior), some number of consecutive observations, and an ending time (immediately after which that water was not an interior water). If an interior water molecule was observed in only one coordinate frame, the event was given a lifetime of 40 ps, the "sampling period" for coordinate sets used in the Voronoi analysis. If the same water molecule was observed to be interior at two successive times, the event was given a lifetime of 80 ps, and so on. This does not, of course, account for the possibility that water molecules might have come and gone and returned between sampling periods. The number of water penetration events observed per picosecond is shown in Figure 20, where, again, one can see that it follows the trend PLA > PVL > PE. Normalized as above to account for differences in the volumes of the star polymers, the trend is only slightly different (PLA > PVL ≫ PE). Histograms giving the fraction of events as a function of their lifetimes are shown in Figure 21, where it can be seen that by far most penetration events last for only one sampling.

There were rare but notable instances of water molecules existing in clusters, for example, as water dimers or trimers. The average number of water clusters per configuration is shown in Figure 18 along with the average number of water molecules observed. When nearly all observed water occurred as monomers, as for the PE star, these curves lay over each other. The size distribution for these clusters is shown in the

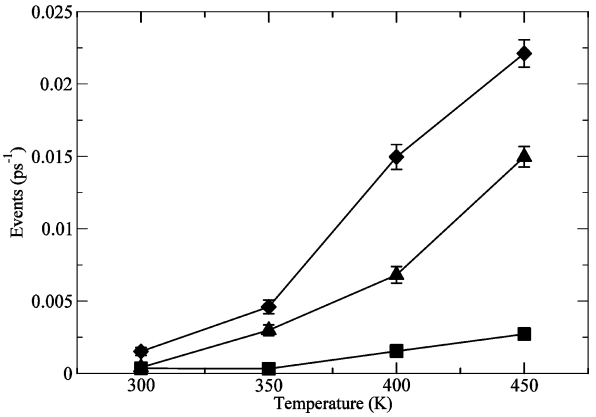

Figure 20. Number of water penetration events observed per picosecond for PLA (diamond), PVL (triangle), and PE (square) star polymers. Uncertainty estimates are ±1 standard deviation.

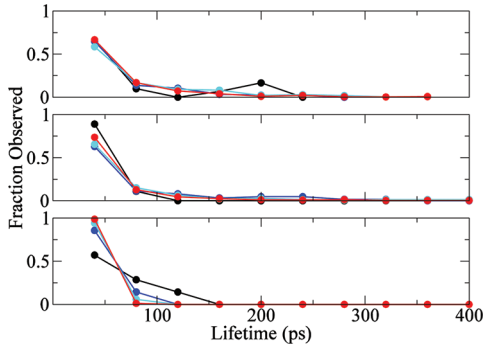

Figure 21. Water penetration lifetime distributions. Top panel is for PLA, middle for PVL, and bottom for PE star polymers. In each case, the data represent the fraction of water penetration events lasting various amounts of time for 300 K (black), 350 K (blue), 400 K (cyan), and 450 K (red).

bar charts in Figure 22, where it can be seen that most interior water molecules were monomers and that water trimers were extremely rare.

4. DISCUSSION

This simulation study precedes a series of small angle neutron scattering (SANS) and backscattering spectroscopy (BASIS) experiments to be performed on very similar star copolymer molecules. These experiments are meant to probe the structure, organization, water content, and kinetics of these kinds of star polymers over a range of temperatures and should produce results that can be compared against this study. The predictions are outlined below.

a. Hydrophobic Cores. The hydrophobic cores in these molecules are strongly phase separated from the other material, both from the hydrophilic segments of the strands and from water. Moreover, the hydrophobic regions in each case are relatively rigid, with the PLA and PVL polymers showing glassy (i.e., disordered and slow) behavior and the PE showing crystalline behavior until rather high temperatures. The slow kinetics manifests itself in a difficulty to sample adequately some of the observables for the PLA and PVL star polymers at the lowest temperature studied (300 K) on the 20 ns time scale of the production simulations. Slow kinetic behavior in the hydrophobic core is also apparent from the reorientational correlation functions.

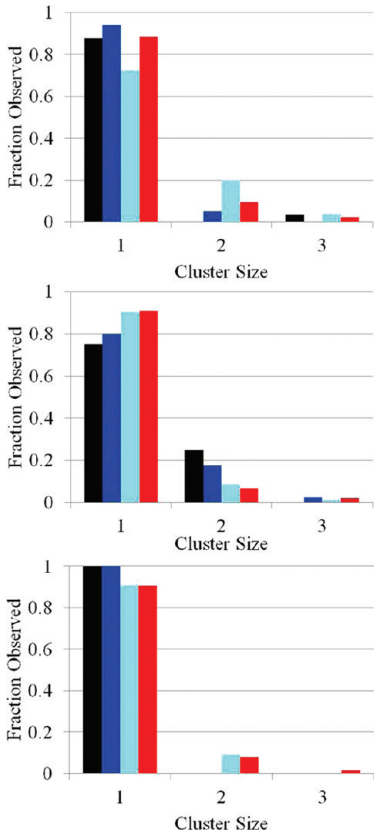

Figure 22. Interior water cluster size histogram. Top panel is for PLA, middle for PVL, and bottom for PE star polymers. In each case, the data represent the fraction of interior water clusters that were water monomers, water dimers, or water trimers for 300 K (black), 350 K (blue), 400 K (cyan), and 450 K (red).

The highly ordered cylindrical structure of the PE star polymer that persists even at 350 K is quite striking given that the 16 arms are more or less symmetrically placed around the adamantane in a way that should destabilize this kind of structure. We note that the structures formed at low temperatures by the polyethylene in the PE star are reminiscent of the structures formed in aqueous solvent by attached alkane chains on the surface of gold nanoparticles.[8]

Further evidence of the solid-like behavior of these molecules is that the surfaces of the hydrophobic regions are highly irregular showing asymmetry, pits, and grooves. The solid behavior persists in these materials until temperatures reach 400 K or higher, at which we see much shorter correlation times for structural changes in the hydrophobic region. Of the two glassy polymers, the PLA polymer seems to be more rigid than the PVL, possibly due to some combination of a higher density of ester groups in the PLA, or more flexibility from the larger alkane segment between ester groups in the PVL. This would suggest that one could produce more liquid-like hydrophobic regions in star polymers by placing longer alkane segments between the ester groups. There may be a limit to this since as one approaches very large segments of alkane, one might begin to see the ordered and very solid structures seen in the PE star polymer.

The fact that the rigidity and structure of the hydrophobic regions persist over such a range of temperatures suggests that this is not likely to be an artifact of the force field and model. We note that the glass transition temperatures for bulk long

dx.doi.org/10.1021/ct300188e | J. Chem. Theory Comput. 2012, 8, 3733−3749

chain polymers of the same material as our hydrophobic cores suggest that these regions *could* be glassy in the context of a star polymer, but it is not clear whether or not glass transition temperatures of bulk materials apply for the case of a star polymer, with arms that are short, tethered to common connection points, and in contact with water. In fact, our original expectation was that the hydrophobic regions would be much more fluid-like.

b. Hydrophilic (PEO) Region. The hydrophilic (PEO) regions of all of the star polymers are very disordered and dynamic, exhibiting significant motion on 100 ps time scales even at the lowest temperatures (300 K) studied. This is apparent in the reorientational correlation functions, where one can see the striking behavioral contrast with the hydrophobic regions to which they are connected. The hydrophilic regions are highly solvated with water, and the PEO segments in these simulations appear to prefer contact with water to contact with the hydrophobic core. However, the thermal behavior of the PEO is most interesting and unusual. There is a slight increase in PEO−hydrophobic core interfacial area but a large decrease in PEO−water interfacial area with *increasing* temperatures, suggesting a tendency of the PEO to self-aggregate with increasing temperature, reminiscent of a lower critical solution temperature (LCST) seen in PEO−water mixtures where one can observe a mixture go from a single phase (miscibility) to two phases with increasing temperature. We believe further experimental and simulation studies should be done to investigate this effect.

We note that the hydrophilic (PEO) regions of the diblock arms in our star polymers are very short compared with those in some of the recently synthesized and simulated[15] star polymer systems. Because of this, there is a limit to how large a fraction of the hydrophobic region can be covered by the PEO in our models. The recent work by Huynh et al.[15] has suggested that longer PEO segments would have a greater tendency to protect the hydrophobic region than the relatively short chains of this study. We have not varied the PEO segment length in this study. However, the tendency for association of the PEO with the hydrophobic core in our model appears to be so weak that the chain length may not adversely affect our results for these types of hydrophobic materials. Clearly, there are entropic forces at play in this matter as well, but we speculate that the balance of interactions exhibited by the force field among water, PEO, and hydrophobic material is more likely to affect these observations than the PEO chain length, since stronger or weaker interactions could tip the balance in various directions. Our water model was TIP4P-Ew, whereas the work of Huynh et al. employed the SPC water model, which has a smaller dipole moment. Also, we used a more solvent-polarized model for the PEO than Huynh et al., resulting in a larger partial charge on the PEO oxygen sites. Both of these aspects could serve to increase the solubility of our PEO. Subsequent work might assess the sensitivity to the water and/or star polymer force field of the relative tendency of PEO to associate with itself, with water, or with the hydrophobic material. However, whether there is sensitivity due to chain length, force field, or temperature, this hints that the degree of protection of the hydrophobic core offered by the hydrophilic region, or its thermal dependence, could be engineered by minor changes in chain length and composition.

The trend in affinity of PEO for the hydrophobic core seen in the interfacial surface area (Figure 16; PLA > PVL > PE) suggests that PEO has a greater affinity for ester-rich hydrophobic material than for alkane-rich material, which might not be surprising. We note, however, that some of the trend in Figure 16 is also due to differences in the volumes of the hydrophobic regions, but the conclusions remain the same when this is accounted for.

Similar observations have been made in a different context by other workers. Yang et al.[7] reported on simulations of PE chains and PEO chains attached to gold nanoparticles in an aqueous environment where they found solvation and closer penetration by water near PEO-coated surfaces and greater water exclusion from the PE-coated gold nanoparticles.

c. Interior Water. The orientationally averaged mass density *seems* to suggest that water penetrates rather far into the hydrophobic region of the polymer. However, the Voronoi analysis suggests that this is an illusion created by orientational averaging over the misshapen and rough hydrophobic surface. In fact, there is a very well-defined water−hydrophobic region interface. These observations are consistent with those of Huynh et al.[15]

In spite of the phase separation between hydrophobic and hydrophilic material, there is a very small amount of water that transiently enters the hydrophobic region, with a probability trend of PLA > PVL ≫ PE, showing a decrease with decreasing ester and increasing alkane content. Water penetration increases with temperature and, so, appears to be thermally activated. However, part of this effect may be due to a change in phase as the hydrophobic core becomes more fluid-like at the higher temperatures. The increase in water content with temperature is much greater for PLA. Some of the differences in water uptake seen among star polymers in our simulations can be explained by different sizes and surface areas of the hydrophobic regions of these systems, but the trend remains the same when allowance is made for this.

Analysis of the temporal behavior of water entry into the hydrophobic regions reveals that such events are rather rare, very short-lived, not very deep into the interior (even for our admittedly small polymers), and predominantly involve single water molecules rather than dimers or trimers of water. Because small molecule esters are relatively soluble in water, our expectations were that there would be much more water diffusing into the ester-rich interiors of these star polymers. Apparently, although ester groups interact favorably with water, the interactions among this hydrophobic material are stronger than the water−ester interactions and lead to the expulsion of water. Finally, we feel that there is enough bulk water contact with the hydrophobic material and enough penetration of water that it could help facilitate a slow degradation of the star polymer as well as enable drug release. On the basis of the differences among the star polymers of this study we feel that such attributes might be controllable with changes in polymer composition and topology.

d. Caveats. In most respects, our results are remarkably consistent with the observations of Huynh et al.[15] in their study of 13 different six arm star polymers based on differing lengths of hydrophobic polycaprolactone (PCL) and hydrophilic PEO segments. A direct numerical comparison of our results with theirs is not possible because of a number of differences in the two studies: the numbers of arms, the segment lengths, the connection mechanism, and different metrics for the computation of water contact and interfacial surface area. We note that their studies showed that with an increasing length of PEO segments relative to that of the PCL segment, the fraction of the total hydrophobic surface area that is protected from the

solvent increased from about 60% (short PEO segments) to about 90% (long PEO segments). We did not explore the effects of changing the length of the PEO segment, but our PEO segments appear to be significantly more soluble in water than theirs, resulting in less protection of the hydrophobic region. We would predict that a PCL-based star polymer, with five methylene groups between ester groups, should behave similarly to our PVL star polymer, with four methylene groups.

Because of the internal strain caused by connecting 16 diblock polymer arms to adamantane, we have observed that as one moves from monomer unit to monomer unit along each of the arms the first couple of units are structurally and kinetically constrained until one reaches some transitional units, after which the material begins to behave in a way that is probably more representative of larger star polymers. These transitional units can be identified from an analysis of the orientationally averaged mass distribution function and the reorientational correlation functions, both resolved by a monomeric unit. The transitional units might change somewhat with temperature, moving closer to the core with increasing temperature. Some of our results may be affected by the small size of these star polymer models since the rigid part of the hydrophobic core might provide a template that artificially stabilizes anomalous structures and adversely affects kinetics and sampling. Subsequent work should be performed with longer arms and/or a more extended or realistic core than adamantane to validate or challenge these results. In general, details of our conclusions may depend somewhat on force field parameters, but we feel the general trends with temperature and with composition of the hydrophobic core are realistic.

One might ask whether the simulations were sufficiently long for adequate sampling, especially given that those of Huynh et al. were at least 200 ns per star polymer system. Their study was done on systems at 300 K, and we note that at that temperature we had difficulty with sampling some of the observables for the PLA and PVL star polymers using 20 ns production simulations. However, they noted that although their simulations exceeded 200 ns, most observables were stable after about 15 ns of sampling. Moreover, we feel that at our higher temperatures (350 K, 400 K, and 450 K) we were able to sample adequately due to the shorter correlation times at these temperatures. Except for a few of the observables measured at 300 K, all of our results follow reasonable systematic trends with temperature, and the uncertainty estimates appear to be realistic. That is, simulations at higher temperatures allow us to estimate the temperatures for which we were not able to sample adequately, and to help establish a kind of "glass transition temperature" for the polymer where the relaxation times begin to exceed the production simulation time. In fact, this is part of the basis for our suggestion that these polymers are glassy at 300 K and 350 K.

Our study employed constant volume simulations to mimic canonical (NVT) ensembles, rather than temperature and pressure controlled simulations to mimic isobaric−isothermal (NpT) ensembles. Due to the method of preparation, the density in all of these simulations was designed to be appropriate near 300 K, and consequently slightly too large for the higher temperatures. However, our goal in performing the higher temperature simulations was to assess the stability of our results rather than to represent accurately these higher temperatures. In any case, the higher two temperatures of our study are known to be above the vaporization temperature of the TIP4P-Ew water model. Moreover, the thermal expansion coefficient of water is such that the error in the density is still rather small, provided one remains in the liquid state.

Pressure denaturation is a phenomenon known in protein science where proteins can be unfolded by subjecting them to increased pressure. The exact mechanism of this has been debated, but one suggestion is that increasing the pressure increases the chemical potential of water molecules in the bulk water (i.e., surrounding the protein) and drives them into the interior of the protein, causing disruption of intraprotein hydrogen bonding. If such an effect were operative here, the increased pressure at our higher temperatures might drive water into the hydrophobic interior, and/or cause disruption of PEO−PEO interactions. The Voronoi analysis does indicate a slight increase in water content with temperature that could be pressure-induced, but the water content is so small that this is probably not significant if operating at all. The effect of increased pressure on the high temperature aggregation of the PEO might cause the aggregation phenomenon to shift in our simulations to slightly higher temperatures, and this might be worthy of investigation.

Finally, we note that the thermal control mechanism used in this study could, in principle, affect temporal observables such as correlation times, rates of water penetration events, and water absorption lifetimes. However, we do not expect this to affect the trends we have observed with respect to composition and temperature.

5. CONCLUSION

We have performed molecular dynamics simulations at four different temperatures on three different star polymers, each with 16 linear diblock copolymer arms bonded to a small adamantane core. Across the three star polymer types, there is a difference in the degree of ester versus alkane content in the hydrophobic component of each arm, including one rich in ester content (PLA), one with a mix of ester and alkane content (PVL), and one with pure alkane content (PE). Whereas earlier simulation studies have explored star polymer behavior at a single temperature and investigated the effect of variations in chain number, length, and composition, but for a given type of hydrophilic and hydrophobic material, we have looked at thermal effects and considered three different types of hydrophobic material.

In all situations, there is a pronounced phase separation of the alkane (PE) and ester (PLA, PVL) hydrophobic material from the rest, producing a phase with virtually no water, and with no mixing with the hydrophilic (PEO) material. The hydrophilic material mixes very well with the water at low temperatures but exhibits signs of phase separation itself at higher temperatures, reminiscent of a lower critical solution temperature (LCST) effect also seen in PEO−water mixtures. At higher temperatures the PEO material condenses and increases its contact with the hydrophobic material.

Structural (density profiles) and kinetic analysis (orientational correlation functions) indicate that the hydrophobic material is solid-like and either very viscous/glassy (ester-based hydrophobic material, PLA, and PVL) or structured (alkane material, PE). The phase separation and solidity of the hydrophobic material in these systems renders them rather impermeable to water, and water entry events are rare, short-lived, and shallow in spite of the fact that the ester-based material has a high density of hydrophilic functional groups.

With respect to the use of these kinds of star polymers as transporters of hydrophobic drug molecules, we feel that the

above observations imply that drug molecule cargos would have a difficult time being absorbed into them and are more likely to be adsorbed onto the hydrophobic surface of these materials, i.e., at either a water−hydrophobic material interface or at a hydrophilic−hydrophobic material interface, rather than being encapsulated in their interiors. If this is the case, we predict drug loading to be proportional to the surface area rather than the volume of the star polymer for star polymers of these compositions.

As evidenced by various shape descriptors and surface area measurements, the surfaces of the hydrophobic regions of our star polymers are generally irregular and misshapen, with grooves and pits. For star polymers with larger hydrophobic regions, there might be a greater tendency to adopt more spherical shapes, but depending on the composition, it is also possible that the hydrophobic surface could have a very rough or fractal nature with a surface area that increases more rapidly than $(\text{volume})^{2/3}$. This, of course, would affect drug loading as well, if it occurs at interfaces. We feel that shape, surface area, and rigidity and their effect on cargo loading will be an important area for experimental characterization.

We believe the tendency for PEO segments to self-aggregate with increasing temperature deserves further experimental and theoretical investigation and could offer a means to control the behavior and function of these types of polymers. In the context of the use of star polymers for drug delivery, an example might be the use of hydrophilic chains engineered in composition and density to increase contact with water when the temperature is lowered slightly, allowing greater exposure of the hydrophobic core and controlled release of cargo stimulated by temperature drop.

AUTHOR INFORMATION

Corresponding Author

*E-mail: swope@almaden.ibm.com.

Present Address

[‖]Department of Physics and Astronomy, University of British Columbia, Vancouver, BC, Canada

Notes

The authors declare no competing financial interest.

ACKNOWLEDGMENTS

A.J.P. was an IBM Distinguished Visiting Scholar, supported by a grant from MacDiarmid Institute for Advanced Materials and Nanotechnology, School of Chemical and Physical Sciences, Victoria University of Wellington, Wellington, New Zealand. A.C.C. was supported by an IBM Predoctoral Fellowship. We would like to thank Wilfred F. van Gunsteren for years of scientific inspiration and friendship and for helping to make science fun.

REFERENCES

(1) Lee, V. Y.; Havenstrite, K.; Tjio, M.; McNeil, M.; Blau, H. M.; Miller, R. D.; Sly, J. Nanogel star polymer architectures: a nanoparticle platform for modular programmable macromolecular self-assembly, intercellular transport, and dual-mode cargo delivery. *Adv. Mater.* **2011**, *23*, 4509.

(2) Appel, E. A.; Lee, V. Y.; Nguyen, T. T.; McNeil, M.; Nederberg, F.; Hedrick, J. L.; Swope, W. C.; Rice, J. E.; Miller, R. D.; Sly, J. Toward biodegradable nanogel star polymers via organocatalytic ROP. *Chem. Commun.* **2012**, DOI: 10.1039/c2cc31406a.

(3) Heise, A.; Hedrick, J. L.; Frank, C. W.; Miller, R. D. Starlike block copolymers with amphiphilic arms as models for unimolecular micelles. *J. Am. Chem. Soc.* **1999**, *121*, 8647−8648.

(4) Srinivas, G.; Pitera, J. W. Soft patchy nanoparticles from solution-phase self-assembly of binary diblock copolymers. *Nano Lett.* **2008**, *8*, 611−618.

(5) Bte, A.; Attia, E.; Ong, Z. Y.; Hedrick, J. L.; Lee, P. P.; Ee, P. L. R.; Hammond, P. T.; Yang, Y.-Y. Mixed micelles self-assembled from block copolymers for drug delivery. *Curr. Opin. Colloid Interface Sci.* **2011**, *16*, 182−194.

(6) Hedrick, J. L.; Trollsås, M.; Hawker, C. J.; Atthoff, B.; Claesson, H.; Heise, A.; Miller, R. D.; Mecerreyes, D.; Jérôme, R.; Dubois, P. Dendrimer-like star block and amphiphilic copolymers by combination of ring opening and atom transfer radical polymerization. *Macromolecules* **1998**, *31*, 8691−8705.

(7) Yang, A.-C.; Weng, C.-I.; Chen, T.-C. Behavior of water molecules near monolayer-protected clusters with different terminal segments of ligand. *J. Chem. Phys.* **2011**, *135*, 034101.

(8) Lane, J. M. D.; Grest, G. S.. Spontaneous asymmetry of coated spherical nanoparticles in solution and at liquid-vapor interfaces. *Phys. Rev. Lett.* **2010**, *104*, 235501.

(9) Grest, G. S.; Fetters, L. J.; Huang, J. S.; Richter, D. Star Polymers: Experiment, Theory and Simulation. In *Advances in Chemical Physics*; Prigogine, E., Rice, S. A., Eds.; John Wiley & Sons: New York, 1996; Vol. *94*, pp 67−163.

(10) Likos, C. N. Effective interactions in soft condensed matter physics. *Phys. Rep.* **2001**, *348*, 267−439.

(11) Ganazzoli, F.; Kuznetsov, Y. A.; Timoshenko, E. G. Conformations of amphiphilic diblock star copolymers. *Macromol. Theory Simul.* **2001**, *10*, 325−338.

(12) Chang, Y.; Chen, W.-C.; Sheng, Y.-J.; Jiang, S.; Tsao, H.-K. Intramolecular janus segregation of a heteroarm star copolymer. *Macromolecules* **2005**, *38*, 6201−6209.

(13) Lee, H.; Larson, R. G. Molecular dynamics study of the structure and interparticle interactions of polyethylene glycol-conjugated PAMAM dendrimers. *J. Phys. Chem. B* **2009**, *113*, 13202−13207.

(14) Lee, H.; Larson, R. G. Effects of PEGylation on the size and internal structure of dendrimers: self-penetration of long PEG chains into the dendrimer core. *Macromolecules* **2011**, *44*, 2291−2298.

(15) Huynh, L.; Neale, C.; Pomes, R.; Allen, C. Systematic design of unimolecular star copolymer micelles using molecular dynamics simulations. *Soft Matter* **2010**, *6*, 5491−5501.

(16) Jorgensen, W. L.; Maxwell, D. S.; Tirado-Rives, J. Development and testing of the OPLS all-atom force field on conformational energetics and properties of organic liquids. *J. Am. Chem. Soc.* **1996**, *118*, 11225−11236.

(17) Price, M. L. P.; Ostrovsky, D.; Jorgensen, W. L. Gas-phase and liquid-state properties of esters, nitriles, and nitro compounds with the OPLS-AA force field. *J. Comput. Chem.* **2001**, *22*, 1340−1352.

(18) Berendsen, H. J. C.; Postma, J. P. M.; van Gunsteren, W. F.; Hermans, J. Interaction Models for Water in Relation to Protein Hydration. In *Intermolecular Forces*; Pullman, B., Ed.; D. Reidel Publishing: Dordrecht, The Netherlands, 1981; p 331.

(19) Huang, C.-F.; Lee, H.-F.; Kuo, S.-W.; Xu, H.; Chang, F.-C. Star polymers via atom transfer radical polymerization from adamantane-based cores. *Polymer* **2004**, *45*, 2261−2269.

(20) Boettcher, C. J. F. *Theory of Electric Polarization*, 2nd ed.; Elsevier: Amsterdam, 1973.

(21) Borodin, O.; Smith, G. D. Development of quantum chemistry force fields for poly(ethylene oxide) with many-body polarization interactions. *J. Phys. Chem. B* **2003**, *107*, 6801−6812.

(22) Ren, P.; Wu, C.; Ponder, J. W. Polarizable atomic multipole-based molecular mechanics for organic molecules. *J. Chem. Theory Comput.* **2011**, *7*, 3143−3161.

(23) Lamoureux, G.; MacKerell, A. D., Jr.; Roux, B. A simple polarizable model of water based on classical Drude oscillators. *J. Chem. Phys.* **2003**, *119*, 5185−5197.

(24) Yu, H. B.; Hansson, T.; van Gunsteren, W. F. Development of a simple, self-consistent polarizable model for liquid water. *J. Chem. Phys.* **2003**, *118*, 221−234.
(25) Rick, S. W.; Stuart, S. J.; Bader, J. S.; Berne, B. J. Fluctuating charge force fields for aqueous solutions. *J. Mol. Liq.* **1995**, *65*, 31−40.
(26) Patel, S.; MacKerell, A. D.; Brooks, C. L., III CHARMM fluctuating charge force field for proteins: II. Protein/solvent properties from molecular dynamics simulations using a nonadditive electrostatic model. *J. Comput. Chem.* **2004**, *25*, 1504−1514.
(27) McAliley, J. H.; Bruce, D. A. Development of force field parameters for molecular simulation of polylactide. *J Chem. Theory Comput.* **2011**, *7*, 3756−3767.
(28) Anderson, P. M.; Wilson, M. R. Developing a force field for simulation of poly(ethylene oxide) based on ab initio calculations of 1,2-dimethoxyethane. *Mol. Phys.* **2005**, *103*, 89−97.
(29) Jaffe, R. L.; Smith, G. D.; Yoon, D. Y. Conformations of 1,2-dimethoxyethane from ab initio electronic structure calculations. *J. Phys. Chem.* **1993**, *97*, 12745−12751.
(30) Smith, G. D.; Jaffe, R. L.; Yoon, D. Y. A force field for simulations of 1,2-dimethoxyethane and poly(oxyethylene) based upon ab initio electronic structure calculations on model molecules. *J. Phys. Chem.* **1993**, *97*, 12752−12759.
(31) Smith, G. D.; Jaffe, R. L.; Yoon, D. Y. Conformations of 1,2-dimethoxyethane in the gas and liquid phase from molecular dynamics simulations. *J. Am. Chem. Soc.* **1995**, *117*, 530−531.
(32) Borodin, O.; Douglas, R.; Smith, G. D.; Trouw, F.; Petrucci, S. Molecular dynamics simulations and experimental study of structure, dynamics and thermodynamics of poly(ethylene oxide) and its oligomers. *J. Phys. Chem. B* **2003**, *107*, 6813−6823.
(33) Borodin, O.; Smith, G. D.; Bandyopadhyaya, R.; Buytner, O. Molecular dynamics study of the influence of solid interfaces on poly(ethylene oxide) structure and dynamics. *Macromolecules* **2003**, *36*, 7873−7883.
(34) Goutev, N.; Ohno, K.; Matsuura, H. Raman spectroscopic study on the conformation of 1,2-dimethoxyethane in the liquid phase and in aqueous solutions. *J. Phys. Chem. A* **2000**, *104*, 9226.
(35) Kriz, J.; Dybal, J. Hydration modes of an amphiphilic molecule 2: NMR, FTIR and theoretical study of the interactions in the system water-1,2-dimethoxyethane. *Chem. Phys.* **2011**, *382*, 104−112.
(36) Swope, W. C.; Horn, H. W.; Rice, J. E. Accounting for polarization cost when using fixed charge force fields. I. Method for computing energy. *J. Phys. Chem. B* **2010**, *114*, 8621−8630.
(37) Swope, W. C.; Horn, H. W.; Rice, J. E. Accounting for polarization cost when using fixed charge force fields. II. Method and application for computing effect of polarization cost on free energy of hydration. *J. Phys. Chem. B* **2010**, *114*, 8631−8645.
(38) Tomasi, J.; Mennucci, B.; Cammi, R. Quantum mechanical continuum solvation models. *Chem. Rev.* **2005**, *105*, 2999−3093.
(39) Horn, H. W.; Swope, W. C.; Pitera, J. W.; Madura, J. D.; Dick, T. J.; Hura, G. L.; Head-Gordon, T. Development of an improved four-site model for biomolecular simulations: TIP4P-Ew. *J. Chem. Phys.* **2004**, *120*, 9665.
(40) Jorgensen, W. L.; Chandrasekhar, J.; Madura, J. D.; Impey, R. W.; Klein, M. L. Comparison of simple potential functions for simulating liquid water. *J. Chem. Phys.* **1983**, *79*, 926.
(41) Abascal, J. L.; Vega, C. A general purpose model for condensed phases of water: TIP4P/2005. *J. Chem. Phys.* **2005**, *123*, 234505.
(42) Plimpton, S. J. Fast parallel algorithms for short-range molecular dynamics. *J. Comput. Phys.* **1995**, *117*, 1−19 . See: http://lammps.sandia.gov (accessed May 2012).
(43) Martyna, G. J.; Tobias, D. J.; Klein, M. L. Constant pressure molecular dynamics algorithms. *J. Chem. Phys.* **1994**, *101*, 4177.
(44) Swope, W. C.; Andersen, H. C.; Berens, P. H.; Wilson, K. R. A computer simulation method for the calculation of equilibrium constants for the formation of physical clusters of molecules: application to small water clusters. *J. Chem. Phys.* **1982**, *76*, 637−649.
(45) Andersen, H. C. Rattle: A velocity version of shake algorithm for molecular dynamics calculations. *J. Comput. Phys.* **1983**, *54*, 24−34.
(46) Hockney, R. W.; Eastwood, J. W. *Computer Simulation Using Particles*; Taylor & Francis: New York, 1989.
(47) Theodorou, D. N.; Suter, U. W. Shape of unperturbed linear polymers: polypropylene. *Macromolecules* **1985**, *18*, 1206.
(48) Notation and formulae related to geometric shape descriptors do not appear to be standardized. We follow Theodorou and Suter[47] where the elements of the gyration tensor are given by $S_{\alpha,\beta} = (1/N) \sum_i \mathbf{r}_{i,\alpha}\mathbf{r}_{i,\beta}$, where the sum is over the N sites $\mathbf{r}_i$ and α and β refer to Cartesian components (x, y, or z); $\mathbf{r}_i$ is measured relative to the center of geometry where $\sum_i \mathbf{r}_{i,\alpha} = 0$. The eigenvalues of S are denoted λ_x, λ_y, and λ_z. The radius of gyration is defined $(R_g)^2 = \lambda_x + \lambda_y + \lambda_z$ and when ordered $\lambda_x < \lambda_y < \lambda_z$. Asphericity is defined as $b = \lambda_z - 0.5(\lambda_x + \lambda_y)$. Acylindricity is defined as $c = (\lambda_y - \lambda_x)$. Shape anisotropy is $\kappa^2 = (b^2 + 0.75c^2)/(R_g)^4$. We report κ^2 and call it anisotropy. Huynh et al.[15] report this as well but call it asphericity . See also http://en.wikipedia.org/wiki/Gyration_tensor (accessed Feb. 2011).
(49) Brostow, W.; Dussault, J. P.; Fox, B. L. Construction of voronoi polyhedra. *J. Comput. Phys.* **1978**, *29*, 81−92.
(50) Finney, J. L. A procedure for the construction of voronoi polyhedral. *J. Comput. Phys.* **1979**, *32*, 137−143.
(51) Connolly, M. L. Solvent-accessible surfaces of proteins and nucleic acids. *Science* **1983**, *221*, 709−713.
(52) Dormidontova, E. E. Influence of end groups on phase behavior and properties of PEO in aqueous solutions. *Macromolecules* **2004**, *37*, 7747−7761.